Non-Fermi-liquid behavior and doping asymmetry in an organic Mott insulator interface

Yoshitaka Kawasugi,[1] Kazuhiro Seki,[1,2,3] Jiang Pu,[4] Taishi Takenobu,[4] Seiji Yunoki,[1,3,5] Hiroshi M. Yamamoto,[1,6] and Reizo Kato[1]

[1]*RIKEN, Wako, Saitama 351-0198, Japan*

[2]*SISSA–International School for Advanced Studies, Via Bonomea 265, 34136 Trieste, Italy*

[3]*RIKEN Center for Computational Science, Kobe, Hyogo 650-0047, Japan*

[4]*Department of Applied Physics, Nagoya University Furo-cho, Chikusa-ku, Nagoya, 464-8603, Japan*

[5]*RIKEN Center for Emergent Matter Science, Wako, Saitama 351-0198, Japan*

[6]*Research Center of Integrative Molecular Systems, Institute for Molecular Science, National Institutes of Natural Sciences, Okazaki, Aichi 444-8585, Japan*

(Received 16 June 2019; revised manuscript received 2 September 2019; published 18 September 2019)

High-T_C superconductors show anomalous transport properties in their normal states, such as the bad-metal and pseudogap behaviors. To discuss their origins, it is important to speculate whether these behaviors are material-dependent or universal phenomena in the proximity of the Mott transition by investigating similar but different material systems. An organic Mott transistor is suitable for this purpose owing to the adjacency between the two-dimensional Mott insulating and superconducting states, simple electronic properties, and high doping/bandwidth tunability in the same sample. Here we report the temperature dependence of the transport properties under electron and hole doping in an organic Mott electric-double-layer transistor. At high temperatures, the bad-metal behavior widely appears except at half filling, regardless of the doping polarity. At lower temperatures, the pseudogap behavior is observed only under hole doping, while the Fermi-liquid-like behavior is observed under electron doping. The bad-metal behavior seems a universal high-energy-scale phenomenon, while the pseudogap behavior is based on lower-energy-scale physics that can be influenced by details of the band structure.

DOI: 10.1103/PhysRevB.100.115141

I. INTRODUCTION

Non-Fermi-liquid behaviors have been observed in the vicinity of two-dimensional Mott insulating and superconducting states in high-T_C cuprates [1–3]. The resistivity ρ increases with temperature far above the Mott-Ioffe-Regel limit and shows T-linear behavior at sufficiently high temperatures (the bad-metal behavior) [4,5]. The Hall coefficient R_H is strongly temperature-dependent despite the metalliclike transport [6,7]. On the other hand, the cotangent of the Hall angle $\rho B/R_H$ (B is magnetic field) is proportional to T^2 as in a Fermi liquid [8]. These anomalies have often been viewed as key unresolved signatures of strong correlation, which is probably relevant to the superconductivity. To discuss their origins, it is important to investigate these behaviors in different systems which can be described with similar models to speculate what behavior is material dependent and what behavior universally appears in the proximity of the Mott transition. Recently, we developed electric-double-layer doping into an organic Mott insulator κ-(BEDT-TTF)$_2$Cu[N(CN)$_2$]Cl (hereafter κ-Cl), resulting in observation of ambipolar superconductivity surrounding the Mott insulating state in one and the same sample [9] [BEDT-TTF = bis(ethylenedithio)tetrathiafulvalene]. Therefore, our organic Mott electric-double-layer transistor (EDLT) would likely show the non-Fermi-liquid behaviors in the normal state. In this study, we investigate the temperature dependence of surface resistivity, the Hall coefficient, and the Hall angle under electron and hole doping in an organic Mott EDLT, with varying doping across half filling in a single sample. At high temperatures, the bad-metal (BM) behavior widely appears except at half filling regardless of the doping polarity. At lower temperatures, the transport properties are highly doing asymmetric; the pseudogap behavior is observed under hole doping, while the Fermi-liquid-like behavior is observed under electron doping. These results imply that the former behavior is a universal high-energy characteristic of the Mott transition, and the latter is a lattice- (band-structure-) dependent phenomenon.

κ-Cl is a two-dimensional organic Mott insulator which comprises alternating layers of conducting BEDT-TTF$^{+0.5}$ radical cations and insulating Cu[N(CN)$_2$]Cl counter anions [10]. The conducting BEDT-TTF molecules are strongly dimerized and can be modeled as a single-band Hubbard model on an anisotropic triangular lattice: $t'/t = -0.44$ [11], where t is the nearest-neighbor hopping and t' is the next-nearest-neighbor hopping. The sign of t'/t is negative, and thus, the Van Hove singularity lies below the Fermi energy (hole-doped side), similar to the high-T_C cuprates, although t' exists only for one diagonal of the dimer sites and, accordingly, the Fermi surface is elliptical (Fig. 1). The BM behaviors are common in normal states of doped cuprates, but field-effect transistors made of κ-Cl showed only insulator-to-metal crossover (IMC) and did not show any BM behavior in our previous experiments, probably because the device conductance comprised both surface and bulk contributions, the latter of which followed only activation-

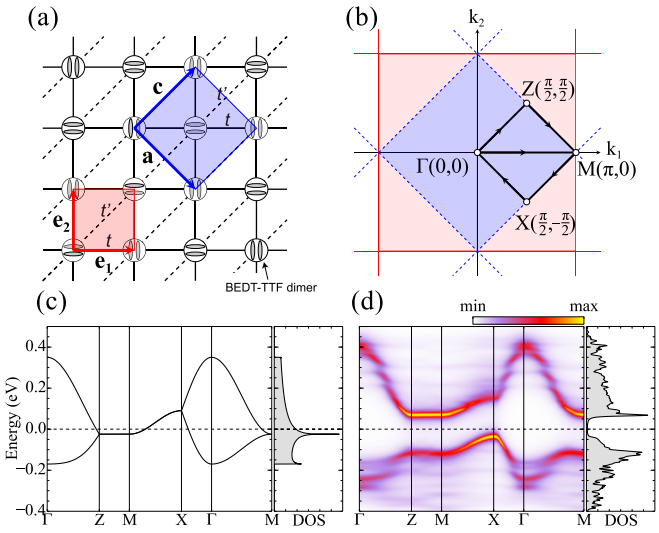

FIG. 1. Unit cells, Brillouin zones, band structure, and single-particle spectral function of κ-Cl. Note that the calculations are based on the one-band model. However, the band structure and spectral functions are shown in the two-site Brillouin zone [blue shaded area in (b)] because the adjacent BEDT-TTF dimers are not completely equivalent in the material. Accordingly, the X, Z, and M points in (c) and (d) correspond to the points $(\pi/2, -\pi/2)$, $(\pi/2, \pi/2)$, and $(\pi, 0)$ in the Brillouin zone of the one-site unit cell. (a) Schematic of the anisotropic triangular lattice of κ-Cl. The translational vectors $\mathbf{e_1}$ and $\mathbf{e_2}$ ($\mathbf{a}$ and $\mathbf{c}$) are represented by the red (blue) arrows. The red (blue) shaded region represents the unit cell containing one site (two sites). The ellipses on the sites denote the conducting BEDT-TTF dimers. (b) The momentum space for the anisotropic triangular lattice. The Brillouin zones of the one- (two-) site unit cell are represented by the red (blue) shaded region bounded by the red solid (blue dashed) lines. (c) Noninteracting tight-binding band structure along highly symmetric momenta and density of states (DOS) of κ-Cl ($t'/t = -0.44$ with $t = 65$ meV). The Fermi level for half filling is set to zero and denoted by dashed lines. (d) Single-particle spectral functions and DOS of κ-Cl at half filling in an antiferromagnetic state at zero temperature, calculated by variational cluster approximation [9]. The Fermi level is denoted by dashed lines at zero energy. The momentum path along Γ-Z-M-X-Γ-M used in (c) and (d) is indicated by arrows in (b).

type temperature dependence [12]. Despite such difficulty in separating the surface conductance from the total one, it is important to reveal whether the BM behaviors exist in the doped organic Mott insulator. A comparison between doped cuprates and κ-BEDT-TTF EDLT, in terms of BM behaviors in the normal states, can address such an issue (Table I).

By using the EDLT method, it is possible to define the charge neutrality point, or the precisely half-filled Mott insulating state, to evaluate the surface transport properties (see Sec. II). In this paper, we show the temperature dependence of surface resistivity ρ_s and the surface Hall coefficient R_{Hs} in the κ-Cl EDLT up to 200 K based on a simple two-fluid (doped surface and undoped bulk) analysis. Note that the strength of correlation U/t of κ-Cl in the present study is larger than those in Ref. [9] because we employed substrates with a lower coefficient of thermal expansion to increase the ratio of surface conductance to bulk conductance. Therefore, the superconductivity does not appear in the present study. In the following, experimental data taken from two samples will be shown; namely, the resistivity data are obtained from sample 1, and the magnetotransport data are obtained from sample 2. The electron and hole doping concentration is changed up to approximately 20% according to the charge displacement current measurements in our previous work [9].

II. METHODS: SAMPLE PREPARATION AND TRANSPORT MEASUREMENT

Thin single crystals of κ-Cl were electrochemically synthesized and laminated on a polyethylene naphthalate (PEN) substrate with patterned Au electrodes (see Fig. S1 in the Supplemental Material [13]). The thicknesses of the crystals measured using a step profiler were 31.5 nm for sample 1 and 81.5 nm for sample 2. Following the laser shaping of the single crystals, we fabricated the EDLT devices by mounting a droplet of the ionic liquid 1-ethyl-3-methylimidazolium 2-(2-methoxyethoxy) ethyl sulfate on a Hall-bar-shaped thin single crystal of κ-Cl and a Au side gate electrode. A 1.2-μm-thick PEN film was then covered for the thinning of the droplet in order to reduce thermal stress at low temperatures. The temperature and magnetic field were controlled using a physical property measurement system (Quantum Design) at sweep rates of 2 K/min ($T > 20$ K), 0.5 K/min ($T < 20$ K), and 150 Oe/s. Throughout the measurements, gate voltage was varied at 220 K because the ionic liquid is solidified at lower temperatures. We measured the transport properties along the a and c axes, which were determined by the shape of the crystal and the sign of the Seebeck effect. In the Hall measurements, the magnetic field was swept in the range of ± 8 T at a constant temperature, and the forward and backward data were averaged to eliminate small linear voltage drifts.

TABLE I. Properties of doped Mott insulators.

	High-T_C cuprates		κ-type BEDT-TTF salts	
	Electron doping	Hole doping	Electron doping	Hole doping
Lattice	Square		Triangular	
t'/t	<0		<0	
Orbital	Cu ($3d$)	O ($2p$)	Upper HOMO	Upper HOMO
Superconductivity	Yes	Yes	Yes [9]	Yes [9,18,19]
Pseudogap	Yes	Yes	No [14]	Yes [14]
Bad-metal behavior	Yes	Yes	Yes (this work)	Yes ([18,19], this work)

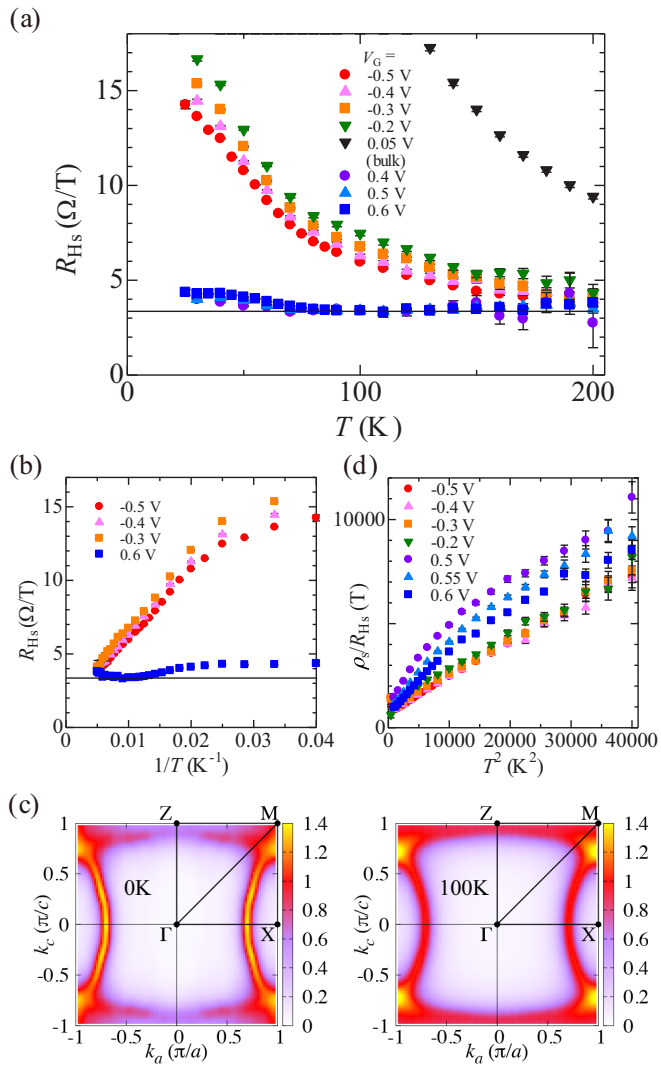

FIG. 2. Hall measurements in sample 2. (a) Temperature dependence of R_{Hs}. The dashed line indicates $1/en_{HF}$, where n_{HF} is the hole density per unit cell at the charge neutrality point. (b) Same as (a), but for R_{Hs} vs $1/T$ plots. (c) CPT calculations of the Fermi surface for 17% hole doping at 0 K (left) and 100 K (right). (d) Hall angle at 1 T vs T^2 plots.

In the EDLT, only the surface of the sample is doped. However, the nondoped region of the sample is also conductive at moderate temperatures ($T \gtrsim 50$ K) in κ-Cl. Assuming two parallel conducting layers, we derived the surface resistivity ρ_s and the surface Hall coefficient R_{Hs} from

$$\rho_s = \left(\frac{1}{\rho} - \frac{1}{\rho_b}\right)^{-1}, \tag{1}$$

$$R_{Hs} = \rho_s^2\left(\frac{R_H}{\rho^2} - \frac{R_{Hb}}{\rho_b^2}\right), \tag{2}$$

where the suffixes b and s denote the bulk and surface, respectively. Here we employed $\rho \times N/(N-1)$ and $R_H \times N/(N-1)$ (N is the number of conducting layers; $N = 21$ and 54 in samples 1 and 2, respectively) at the charge neutrality point as ρ_b and R_{Hb}, respectively (see Fig. S2 in the Supplemental Material [13]). The error bars in Fig. 2 were calculated from the standard deviation of the Hall resistance vs magnetic field plots and the standard error propagation formula. The surface to bulk conductivity ratios in sample 1 were approximately 25%, 19%, 16%, 24% at $V_G = -0.6, -0.3, +0.3, +0.6$ V, respectively.

The variational-cluster-approximation calculations for Fig. 1(d) and cluster-perturbation-theory calculations for Fig. 2(c) were performed for the Hubbard model on an anisotropic triangular lattice ($t'/t = -0.44$, $U/t = 5.5$, and $t = 65$ meV [11]) using a 12-site cluster (an antiferromagnetic insulating state at half filling is assumed in the former case). Details of the calculations are described in our previous paper [9,14].

III. RESULTS

A. Temperature dependence of resistivity

Figure 3(a) shows the temperature T dependence of the surface resistivity ρ_s under electron doping. At high temperatures, metalliclike conduction ($d\rho_s/dT > 0$) above the Mott-Ioffe-Regel limit ρ_{MIR} is observed in a wide range of doping levels. Although the resistivity is not T linear (between linear and quadratic) in this temperature range, this is a BM behavior in the sense that the mean free path of carriers is shorter than the site distance. The power-law exponent α estimated from $\rho_s = \rho_0 + AT^\alpha$ (ρ_0 is the residual resistivity, A is an arbitrary prefactor) is approximately 1.5 between 50 and 200 K at 0.6 V, although the exponent is not very accurate because the effect of thermal contraction (variations of the cell parameters [15]) is not considered here. At 20–50 K, this sample exhibits an IMC at gate voltage $V_G = 0.34$ V; namely, the sign of $d\rho_s/dT$ changes by the gate voltage. The resistivity at 0.34 V is close to h/e^2, which corresponds to ρ_{MIR} for a two-dimensional metal with an isotropic Fermi surface [16,17]. By further electron doping, the temperature dependence of ρ_s approaches that of a Fermi liquid at low temperatures. As shown in Fig. 3(c), ρ_s in the highly electron doped states are almost quadratic in temperature below ~20 K, although they slightly deviate from the T^2 line in the lowest-temperature region because of the weak localization effect.

Under hole doping, the BM behavior is found at high temperatures as in the case of electron doping [Fig. 3(b)]. Although an accurate estimation of the power-low exponent is difficult owing to the resistivity upturn, the temperature dependence of ρ_s appears more T linear than in the case of electron doping at high temperatures [Fig. 3(d)]. This is consistent with the T-linear resistivity in the hole-doped compound κ-(BEDT-TTF)$_4$Hg$_{2.89}$Br$_8$ at high temperatures [18,19]. The gate voltages where the BM behavior occurs ($|V_G| \sim 0.1$ V) correspond to a few percent doping according to the Hall effect. On the other hand, no IMC with varying V_G is observed at low temperatures.

Figure 3(e) shows color plots of more detailed ρ_s data under electron doping. The result of calculations based on dynamical mean-field theory (DMFT) [20] is also shown as a reference. The results of our experiment and the DMFT calculations are qualitatively similar at high temperatures but somehow different at low temperatures: the high-resistance region in the experiment gradually expands with decreasing

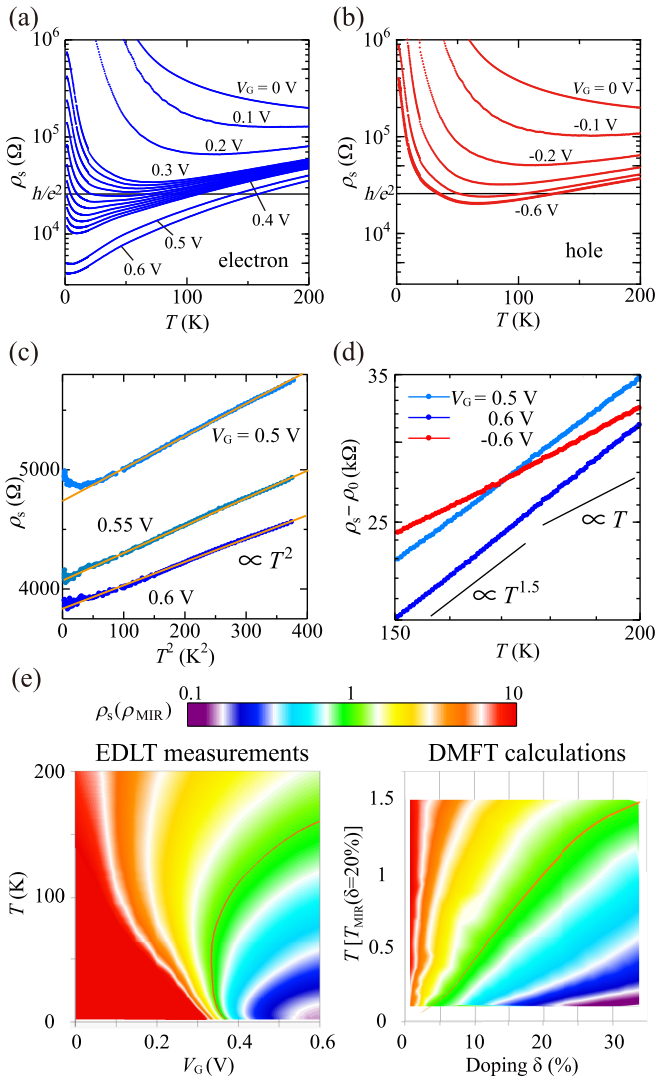

FIG. 3. Temperature T dependence of surface resistivity ρ_s along the a axis in sample 1 under (a) electron doping and (b) hole doping. (c) ρ_s vs T^2 plots below 20 K for $V_G = +0.5$, $+0.55$, and $+0.6$ V. The orange solid lines denote $\rho_s \propto T^2$ lines. (d) Log-log plots of $\rho_s - \rho_0$ vs T for $V_G = +0.5$ and $+0.6$ V. The plot for -0.6 V is also shown as a reference, where ρ_0 at $+0.6$ V is assumed. (e) Color plots of surface resistivity under electron doping. The original data (52 temperature cycles at different V_G values) are shown in Fig. S3 in the Supplemental Material [13]. The orange solid line indicates the contour line ρ_{MIR}. The right panel shows the results of DMFT calculations in Ref. [20], where the temperature is normalized by T_{MIR}, the temperature at which the resistivity reaches ρ_{MIR} for $\delta = 20\%$.

temperature because of Anderson localization. As a result, the ρ_{MIR} line is shifted to a higher doping level and becomes almost vertical in the temperature range 20–50 K. The IMC at $V_G = 0.34$ V is therefore related not only to the electron correlation but also to the surface potential disorder.

B. Temperature dependence of Hall coefficient and Hall angle

In a Fermi liquid with a single type of carrier, $1/eR_H$ denotes the carrier density corresponding to the volume enclosed

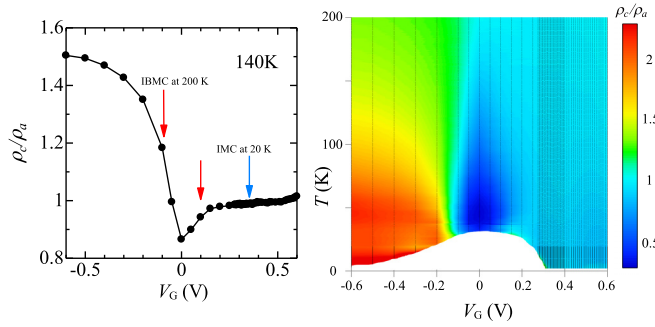

FIG. 4. Temperature dependence of in-plane anisotropy of surface resistivity in sample 1 (note that both a and c axes are parallel to the conducting plane in this material). The black dots denote the data points in both panels. The left panel shows the height profile at 140 K where IBMC (indicated by red arrows) and IMC (blue arrow) denote insulator-to-BM crossover and insulator-to-metal crossover, respectively. Data are missing at low temperatures and low doping (white region in the right panel) due to the high resistance.

by the Fermi surface (FS) [21]. If the doping-driven Mott transition restores the noninteracting FS topology, $1/eR_H$ coincides with the intrinsic carrier density, $1 - \delta$ hole per site, where δ is the electron doping concentration. This is applicable to the case of surface electron doping. Here $1/eR_{Hs}$ is close to the half-filled carrier density (one hole per site) and almost linearly decreases with V_G. By contrast, $1/eR_{Hs}$ under hole doping is several times less than $1 - \delta$ at low temperature, as previously reported [14]. This is attributed to the emergence of an anisotropic pseudogap near the saddle points of the band dispersion that cause the Van Hove singularity [the saddle points locate at the same wave vectors as those of the cuprates, $(\pm\pi, 0)$ and $(0, \pm\pi)$ in the single-band model, as shown in Fig. 1] [14]. The noninteracting ellipsoidal FS is truncated, and $1/eR_{Hs}$ reflects the volume of the lenslike hole pocket [22].

The temperature dependences of R_{Hs} in Fig. 2(a) display the features described above. Moreover, our experiment finds that R_{Hs} is almost temperature independent under electron doping, while it significantly decreases with temperature under hole doping [and appears proportional to $1/T$ above ~50 K, as shown in Fig. 2(b)], as if the pseudogap diminishes and the noninteractinglike FS starts to contribute to R_{Hs} with increasing temperature. Our finite-temperature cluster-perturbation-theory (CPT) calculations [23] also support the diminishment of the pseudogap with temperature [Fig. 2(c)].

Figure 2(d) shows the surface Hall angle at 1 T ρ_s/R_{Hs} (the inverse Hall mobility) vs T^2. In the hole-doped states, ρ_s/R_{Hs} is nearly quadratic in temperature with nonzero intersections. The slope does not depend much on V_G, whereas the y-axis intersection, i.e., ρ_s/R_{Hs} at $T = 0$, decreases with doping. By contrast, the quadratic relation is less applicable in the electron-doped states. Although the quadratic relation is suggested at low temperatures, in agreement with the Fermi-liquid behavior [Fig. 3(c)], the plots bend downward at approximately 100 K, and the slope becomes more V_G independent above this temperature.

TABLE II. Transport properties of the κ-Cl EDLT in this work. The power-law exponents of the BM behaviors are roughly estimated values assuming constant cell parameters.

	Electron doping		Hole doping	
	High T	Low T	High T	Low T
Resistivity	Bad metal ($\propto T^{1.5}$)	Fermi liquid ($\propto T^2$)	Bad metal ($\propto T$)	Semiconductor
Hole density per site	$1-\delta$	$1-\delta$	Activated up to $1-\delta$	$\sim(1-\delta)/3$
Hall angle	Nonquadratic	$\propto T^2$	$\propto T^2$	
Fermi surface (CPT)	Elliptical	Elliptical	Elliptical	Lenslike (pseudogap)
Resistivity anisotropy	Low	Low	Medium	High
Superconductivity	Yes (first-order-like, narrow V_G region) [9]		Yes (wide V_G region) [9]	

C. Temperature dependence of resistivity anisotropy

Figure 4 shows the in-plane anisotropy of the surface resistivity ρ_c/ρ_a up to 200 K. Here ρ_c (ρ_a) denotes the surface resistivity along the c axis [a axis; the short axis of the elliptical FS is parallel to the c axis, as shown in Fig. 2(c)]. The color plots visually show the three domains, namely, the electron-doped, hole-doped, and Mott insulating states. They are separated at low doping levels $|V_G| \sim 0.1$ V, which is in agreement with the occurrence of the BM behavior in Fig. 3. The value of ρ_c/ρ_a is highest in the hole-doped state, followed by the electron-doped (most isotropic) and the Mott insulating states. ρ_c/ρ_a is less than 1 in the Mott insulating state, as predicted by the conductivity calculations in our previous study [14], although it is not clear why ρ_c/ρ_a is much less than that in the electron-doped state. As shown in the previous report [14], the increase in ρ_c/ρ_a under hole doping is attributable to the pseudogap formation that suppresses the carrier conduction along the c axis. At any gate voltage, the resistivity becomes more isotropic with increasing temperature, probably because the pseudogap diminishes due to thermal fluctuation at high temperatures, as implied by the temperature dependence of R_{Hs} and the CPT calculations. However, the in-plane anisotropy in the hole-doped side remained even at 200 K. All of the measurements are briefly summarized in Table II, and the summarizing phase diagram is shown in Fig. 5.

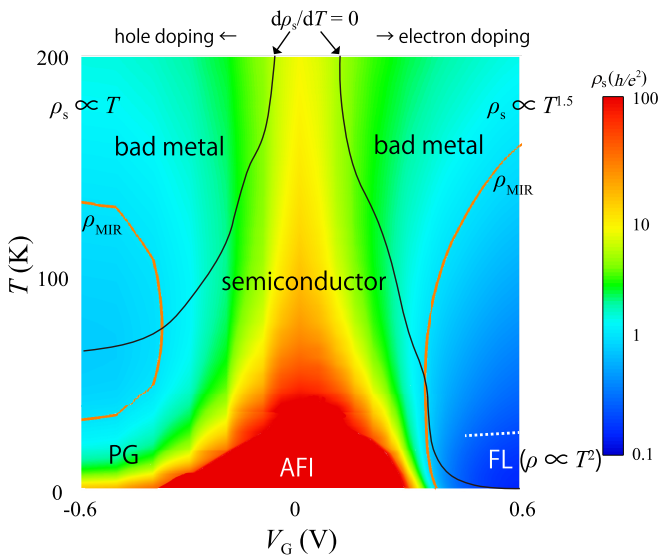

FIG. 5. Phase diagram drawn from the transport properties of sample 1. PG, AFI, and FL denote pseudogap, antiferromagnetic insulator, and Fermi liquid, respectively. Black lines indicate temperatures where $d\rho_s/dT = 0$. Above this temperature, the conductivity is metallicelike. Orange lines indicate temperatures and V_G where $\rho_s = \rho_{MIR}$. The surface resistivity is quadratic in temperature below the white dashed line on the electron-doped side. The surface resistivity ρ_s is shown as a color plot.

IV. DISCUSSION

Recently, we observed ambipolar superconductivity in a strain-tuned organic Mott EDLT based on κ-Cl [9]. The results described here have been measured in the same device with slightly larger tensile strain, or U/t. Therefore, the BM and non-Fermi-liquid behaviors observed in the transport properties of samples 1 and 2 are in close proximity to the superconducting states. This type of band-filling control experiment with tunable U/t in the proximity of the superconducting phase has become possible by utilizing a flexible organic lattice with a bendable substrate. Determining the details of the phase diagram such as the existence or absence of a possible quantum critical point will become possible in future works, although the present measurement points are not finely enough tuned because of the limitation of EDLT.

The BM behavior is suggested by various numerical studies [20,24–26]. The DMFT calculations [20], for example, show that the BM behavior appears as a result of the Mott quantum criticality in the crossover region. Besides such deductive rationalization, an inductive extraction of BM behavior from experiments with different materials is also important [27–29] because extrinsic factors not related to a pure Mott insulator should be excluded. Our present results have clearly confirmed the emergence of the BM behavior in the doped organic Mott insulator, κ-BEDT-TTF EDLT.

According to the Hall measurements, hole-doped κ-Cl resembles lightly or optimally hole doped cuprates such as $La_{2-x}Sr_xCuO_4$ [7]. The strongly temperature dependent R_{Hs} (which appears proportional to $1/T$ at high temperatures) and the quadratic-in-temperature Hall angle in κ-Cl are also in common with the so-called strange-metal phase in hole-doped cuprates. This analogy supports the presence of a pseudogap in hole-doped κ-Cl.

On the other hand, electron-doped κ-Cl appears quite different from electron-doped cuprates. In particular, the value and even the sign of R_H in electron-doped cuprates are generally temperature dependent and are uncorrelated to the volume

of the noninteracting holelike Fermi surface [30]. This is in contrast to electron-doped κ-Cl, which shows almost temperature independent R_{Hs} simply corresponding to the noninteracting Fermi surface with hole density $1-\delta$. Its transport properties are rather similar to those of the over-hole-doped cuprates such as $La_{2-x}Sr_xCuO_4$ [5,7] and $Tl_2Ba_2CuO_{6+\delta}$ [31], where the resistivity is proportional to $\sim T^{\alpha}$ with α between 1 and 2, R_{H} corresponds to the large holelike Fermi surface, and the Hall angle vs T^2 plots bend downward.

The similarities in the hole-doped states and differences in the electron-doped states between κ-Cl and cuprates indicate the difference in their doping asymmetry. In κ-Cl, electron doping induces more drastic transitions in resistivity compared to hole doping. Similar doping asymmetry has also been observed for the superconducting region in the strain-controlled EDLT [9]. Unlike hole-doped superconductivity, electron-doped superconductivity shows a very abrupt and discontinuous (first-order-like) transition. Although the first-order transitions are not observed in this study, they may appear at extremely low temperatures because of large U/t, as shown by the DMFT calculations [20]. This asymmetry may be attributable to the difference in their noninteracting band structures and resultant single-particle spectral functions in the Mott insulating state, where t' exists only for one diagonal (κ-Cl) or for both diagonals (cuprates) of the sites.

To summarize, we investigated the surface transport properties of the EDLT based on an organic Mott insulator κ-Cl, which forms an anisotropic triangular lattice and has Van Hove singularity below the Fermi level (hole-doped side) in the noninteracting band structure. In the hole-doped state, non-Fermi-liquid behaviors such as the BM behavior, strongly temperature-dependent R_{Hs}, and the quadratic-in-temperature Hall angle are observed, similar to the strange metal phase in hole-doped cuprates. On the other hand, the doping asymmetry in κ-Cl appears different from that in cuprates: the transport properties of electron-doped κ-Cl are similar to heavily hole doped cuprates and are not likely to be related to those of electron-doped cuprates. Electron-doped κ-Cl shows more Fermi-liquid-like behaviors such as the quadratic-in-temperature resistivity at low temperatures and the temperature-independent R_{H} nearly corresponding to the large noninteracting Fermi surface. The difference in the doping asymmetry between κ-Cl and cuprates may originate from the difference in their band structures. At high temperatures, the BM behavior widely appears in κ-Cl regardless of the doping polarity, supporting the universality of the BM transport near the Mott transitions. Even in the sufficiently electron doped state, which shows Fermi-liquid behavior at low temperatures, the system still shows the BM behavior at high temperatures, probably because of the proximity effects of the Mott quantum criticality.

Finally, we emphasize that determination of physical properties in a wide range of thermodynamic parameters in a single sample is quite important for understanding Mott physics. Because of its low half-filling carrier density, κ-Cl is one of the most appropriate materials to study Mott physics in wide filling control using the field effect without electrical breakdown or electrochemical degradation. We have found that the BM behavior at high temperatures persists at almost all doping levels, while the pseudogap behavior at low temperatures is quite band structure dependent, implying the different energy scales and mechanisms governing these two behaviors.

ACKNOWLEDGMENTS

We thank Dr. V. Dobrosavljević for discussions. We would like to acknowledge Teijin DuPont Films Japan Limited for providing the PET films. This work was supported by MEXT and JSPS KAKENHI (Grants No. JP16H06346, JP15K17714, JP26102012, JP25000003, and JP16H4140), JST ERATO, MEXT Nanotechnology Platform Program (Molecule and Material Synthesis), and MEXT HPCI Strategic Programs for Innovative Research (SPIRE) (Grants No. hp140128 and hp150112). We are also grateful for allocation of computational time of the HOKUSAI GreatWave and HOKUSAI BigWaterfall supercomputer at RIKEN Advanced Center for Computing and Communication (ACCC) and the K computer at RIKEN Center for Computational Science (R-CCS). K.S. acknowledges support from the Overseas Research Fellowship Program of the Japan Society for the Promotion of Science.

[1] E. Dagotto, Rev. Mod. Phys. **66**, 763 (1994).
[2] M. Imada, A. Fujimori, and Y. Tokura, Rev. Mod. Phys. **70**, 1039 (1998).
[3] P. A. Lee, N. Nagaosa, and X.-G. Wen, Rev. Mod. Phys. **78**, 17 (2006).
[4] M. Gurvitch and A. T. Fiory, Phys. Rev. Lett. **59**, 1337 (1987).
[5] H. Takagi, B. Batlogg, H. L. Kao, J. Kwo, R. J. Cava, J. J. Krajewski, and W. F. Peck, Jr., Phys. Rev. Lett. **69**, 2975 (1992).
[6] S.-W. Cheong, S. E. Brown, Z. Fisk, R. S. Kwok, J. D. Thompson, E. Zirngiebl, G. Gruner, D. E. Peterson, G. L. Wells, R. B. Schwarz, and J. R. Cooper, Phys. Rev. B **36**, 3913 (1987).
[7] Y. Ando, Y. Kurita, S. Komiya, S. Ono, and K. Segawa, Phys. Rev. Lett. **92**, 197001 (2004).
[8] T. R. Chien, Z. Z. Wang, and N. P. Ong, Phys. Rev. Lett. **67**, 2088 (1991).
[9] Y. Kawasugi, K. Seki, S. Tajima, J. Pu, T. Takenobu, S. Yunoki, H. M. Yamamoto, and R. Kato, Sci. Adv. **5**, eaav7282 (2019).
[10] J. Williams, A. Kini, H. Wang, K. D. Carlson, U. Geiser, L. Montgomery, G. Pyrka, D. Watkins, and J. Kommers, Inorg. Chem. **29**, 3272 (1990).
[11] H. C. Kandpal, I. Opahle, Y.-Z. Zhang, H. O. Jeschke, and R. Valentí, Phys. Rev. Lett. **103**, 067004 (2009).
[12] Y. Sato, Y. Kawasugi, M. Suda, H. M. Yamamoto, and R. Kato, Nano Lett. **17**, 708 (2017).
[13] See Supplemental Material at http://link.aps.org/supplemental/10.1103/PhysRevB.100.115141 for experimental details and additional data.

[14] Y. Kawasugi, K. Seki, Y. Edagawa, Y. Sato, J. Pu, T. Takenobu, S. Yunoki, H. M. Yamamoto, and R. Kato, Nat. Commun. **7**, 12356 (2016).
[15] J. Müller, M. Lang, F. Steglich, J. A. Schlueter, A. M. Kini, and T. Sasaki, Phys. Rev. B **65**, 144521 (2002).
[16] D. C. Licciardello and D. J. Thouless, Phys. Rev. Lett. **35**, 1475 (1975).
[17] K. Ahadi, O. F. Shoron, P. B. Marshall, E. Mikheev, and S. Stemmer, Appl. Phys. Lett. **110**, 062104 (2017).
[18] H. Taniguchi, T. Okuhata, T. Nagai, K. Satoh, N. Môri, Y. Shimizu, M. Hedo, and Y. Uwatoko, J. Phys. Soc. Jpn. **76**, 113709 (2007).
[19] H. Oike, K. Miyagawa, H. Taniguchi, and K. Kanoda, Phys. Rev. Lett. **114**, 067002 (2015).
[20] J. Vučičević, D. Tanasković, M. J. Rozenberg, and V. Dobrosavljević, Phys. Rev. Lett. **114**, 246402 (2015).
[21] J. M. Luttinger, Phys. Rev. **119**, 1153 (1960).
[22] K. Oshima, T. Mori, H. Inokuchi, H. Urayama, H. Yamochi, and G. Saito, Phys. Rev. B **38**, 938 (1988).
[23] K. Seki, T. Shirakawa, and S. Yunoki, Phys. Rev. B **98**, 205114 (2018).
[24] X. Deng, J. Mravlje, R. Žitko, M. Ferrero, G. Kotliar, and A. Georges, Phys. Rev. Lett. **110**, 086401 (2013).
[25] W. Xu, K. Haule, and G. Kotliar, Phys. Rev. Lett. **111**, 036401 (2013).
[26] J. Kokalj, Phys. Rev. B **95**, 041110(R) (2017).
[27] A. W. Tyler, A. P. Mackenzie, S. Nishizaki, and Y. Maeno, Phys. Rev. B **58**, R10107(R) (1998).
[28] M. M. Qazilbash, K. S. Burch, D. Whisler, D. Shrekenhamer, B. G. Chae, H. T. Kim, and D. N. Basov, Phys. Rev. B **74**, 205118 (2006).
[29] P. Limelette, P. Wzietek, S. Florens, A. Georges, T. A. Costi, C. Pasquier, D. Jérome, C. Mézière, and P. Batail, Phys. Rev. Lett. **91**, 016401 (2003).
[30] N. P. Armitage, P. Fournier, and R. L. Greene, Rev. Mod. Phys. **82**, 2421 (2010).
[31] A. P. Mackenzie, S. R. Julian, D. C. Sinclair, and C. T. Lin, Phys. Rev. B **53**, 5848 (1996).